Acta Pharmaceutica Sinica B 2023;13(12):5016–5029

Chinese Pharmaceutical Association
Institute of Materia Medica, Chinese Academy of Medical Sciences

Acta Pharmaceutica Sinica B

www.elsevier.com/locate/apsb
www.sciencedirect.com

ORIGINAL ARTICLE

Reactive oxygen species and nitric oxide scavenging nanoparticles alleviating rheumatoid arthritis through adjusting the seeds and growing soils

Peng Hua[a,†], Ruifeng Liang[a,†], Yanbei Tu[a], Yuying Yin[a], Man-Kay Law[b], Meiwan Chen[a,*]

[a]*State Key Laboratory of Quality Research in Chinese Medicine, Institute of Chinese Medical Sciences, University of Macau, Macau SAR, China*
[b]*State Key Laboratory of Analog and Mixed-Signal VLSI, IME and FST-ECE, University of Macau, Macau SAR, China*

Received 24 April 2023; received in revised form 16 July 2023; accepted 20 July 2023

KEY WORDS

Bilirubin;
o-Phenylenediamine;
Notopterol;
ROS and NO scavenging;
JAK-STAT pathway;
Anti-inflammatory;
Cartilage protection;
Rheumatoid arthritis

Abstract Normalizing inflamed soils including reactive oxygen species (ROS), nitric oxide (NO), cell-free DNA, and regulating inflammation-related seeds such as macrophages, neutrophils, fibroblasts, represent a promising strategy to maintain synovial tissue homeostasis for rheumatoid arthritis (RA) treatment. Herein, ROS scavenging amphiphilic block copolymer PEGylated bilirubin and NO-scavenging PEGylated *o*-phenylenediamine were fabricated to self-assemble into a dually responsive nanoparticle loaded with JAK inhibitor notopterol (Not@BR/oPDA-PEG, NBOP NPs). The simultaneous ROS and NO depletion combined with JAK-STAT pathway inhibition could not only promote M2 polarization to reduce further ROS and NO generation, but also decrease cytokines and chemokines to prevent immune cell recruitment. Specifically, NBOP NPs responded to high level ROS and NO, and disintegrated to release notopterol in inflamed joints as the hydrophobic heads BR and oPDA were transformed into hydrophilic ones. The released notopterol could inhibit the JAK-STAT pathway of inflammatory cells to reduce the secretion of pro-inflammatory cytokines and chemokines. This strategy represented an effective way to regulate RA soils and seeds through breaking the positive feedback loop of inflammation

*Corresponding author.
E-mail address: mwchen@um.edu.mo (Meiwan Chen).
[†]These authors made equal contributions to this work.
Peer review under responsibility of Chinese Pharmaceutical Association and Institute of Materia Medica, Chinese Academy of Medical Sciences.

https://doi.org/10.1016/j.apsb.2023.07.021

aggravation, achieving an excellent anti-RA efficacy in a collagen-induced arthritis rat model. Taken together, our work offered a reference to adjust RA soils and seeds for enhanced RA treatment.

1. Introduction

Rheumatoid arthritis (RA) is an autoimmune disease characterized by systemic inflammation and synovial hyperplasia, which gradually impairs the patient's joint function and eventually leads to disability[1,2]. Although non-steroidal anti-inflammatory drugs (NSAIDs), glucocorticoids (GCs), disease-modifying anti-rheumatic drugs (DMARDs) and biologics are widely employed in clinics to treat RA, most of the agents are far from satisfactory due to the limited therapeutic efficacy, poor bioavailability and severe side effects[3–5]. Emerging strategies for treating RA mainly focused on normalizing RA soils including superfluous reactive oxygen species (ROS)[6], nitric oxide (NO)[7], cell-free DNA[8], hypoxia[9] as well as adjusting RA seeds such as endothelial cells[10], fibroblasts[11], and immune cells[12]. The RA soils are generated or formed as a result of the RA seeds, which in turn regulate cell behavior as the rich source of biochemical signals. For instance, pro-inflammatory M1 macrophages constantly produce ROS and NO while the high level of ROS and NO further induce the activation of M1 macrophages. Excessive ROS production increases the inflammatory cytokines such as tumor necrosis factor-α (TNF-α), interleukin-1β (IL-1β), and interleukin-6 (IL-6), which accelerate the progression of RA[13,14]. In addition, the high level of NO produced by activated macrophages plays an essential role in the inflammatory cascade as a pro-inflammatory mediator[15]. On the other hand, RA-related cells comprising of macrophages, endothelial cells, fibroblasts, neutrophils and so on, act as seeds and collectively participate in RA progression. To adjust RA seeds, regulating Janus kinase-signal transducer and activator of transcription (JAK-STAT) signaling pathway are promising in RA treatment by reducing pro-inflammatory cytokine and chemokine generation in inflammatory cells[16]. The recruited macrophages in the RA joint are mainly polarized to the M1 phenotype to generate ROS and NO and secret cytokines and chemokines, inevitably posing a positive feedback loop to aggravate inflammation. Thus, ROS/NO scavenging combined with JAK-STAT inhibition can be considered as a promising strategy to simultaneously adjust the seeds and growing soils for RA therapy.

Nanomaterials have been regarded as potential platforms to deliver multiple therapeutic agents for cocktail therapy. Recently, rational-designed nano delivery systems have been fabricated to regulate RA soils and seeds. However, such all-in-one nanomedicine hardly realizes diverse spatiotemporal delivery patterns of agents compared with stimuli-responsive nanotherapeutics. In fact, the delivery of different agents into corresponding therapeutic action sites can further enhance the efficacy of regulating the soil and seeds. Moreover, nanomaterials can be rationally modified to regulate RA soils by scavenging ROS and NO. For instance, Huang and co-workers constructed ROS-responsive nanoparticles based on 4-phenylboronate-conjugated cyclodextrin, which can effectively deplete ROS in RA and significantly enhance the anti-inflammatory effect of loaded dexamethasone[17]. Kim et al[18]. rationally designed an injectable *in situ* polymerized aggregate hybrid gel platform for NO scavenging and sequential drug release. Nevertheless, there is still a lack of biomaterials for enabling ROS and NO depletion simultaneously with high stability and low off-target toxicity.

In view of this, we fabricated dually ROS and NO responsive nanoparticles by taking advantage of the efficient ROS depletion capacity of endogenous compound bilirubin (BR) and NO-scavenging compound molecule *o*-phenylenediamine (*o*PDA). Two linear amphiphilic block polymers, BR-PEG and *oPDA*-PEG were constructed by covalently attaching BR and *o*PDA to polyethylene glycol (PEG) to self-assemble into nanoparticles (Not@BR/*o*PDA-PEG, NBOP NPs, Scheme 1). The natural product-derived JAK-STAT inhibitor notopterol was encapsulated to regulate inflammatory cells[19]. Specifically, NBOP NPs could passively target the inflammatory microenvironment by extravasation through leaky vasculature and subsequent inflammatory cell-mediated sequestration (ELVIS) effect. Upon reaching the inflammatory environment of the joint with high level ROS and NO, BR and *o*PDA at the hydrophobic end of the polymer could efficiently consume ROS and NO, respectively. The hydrophobic part was oxidized to hydrophilic compounds, resulting in the disintegration of NBOP to release Not. NBOP NPs not only downregulated ROS and NO for converting macrophage to M2 type, but also relieved inflammation by downregulating pro-inflammatory cytokines and chemokines. The strategy of adjusting RA growing soils (ROS/NO scavenging) and seeds (JAK-STAT inhibition) could provide insights for developing efficient combination therapy of RA.

2. Materials and methods

2.1. Materials

Notopterol was purchased from Chengdu Yirui Biotechnology Co., Ltd. (Chengdu, China). *N*-Hydroxy succinimide, *o*-phenylenediamine, $mPEG_{2000}$-SH, $mPEG_{2000}$-NH_2, isocyanoethyl methacrylate, DiR, coumarin 6, tetrahydrofuran and benzoin dimethyl ether was purchased from Macklin Co., Ltd. (Shanghai, China). Bilirubin was obtained from Yuanye Biological Technology Co., Ltd. (Shanghai, China). 1-(3-Dimethylaminopropyl)-3-ethylcarbodiimide hydrochloride, acetonitrile and dimethyl sulfoxide were obtained from Aladdin Biochemical Technology Co., Ltd. (Shanghai, China). Chloroform, ether and hydrochloric acid were obtained from Guangzhou Chemical Reagent Factory (Guangzhou, China). Lipopolysaccharide (LPS) was obtained from Biosharp (Hefei, China). Methanol was purchased from Xilong Scientific Co., Ltd. (Shantou, China). 2′,7′-Dichlorodihydrofluorescein diacetate (DCFH-DA), 3-amino, 4-aminomethyl-2′,7′-difluorescein, diacetate (DAF-FM DA), hydrogen peroxide assay kit and nitric oxide assay kit were obtained from Beyotime Biotechnology (Shanghai, China). Rat TNF-α, IL-6 and IL-1β

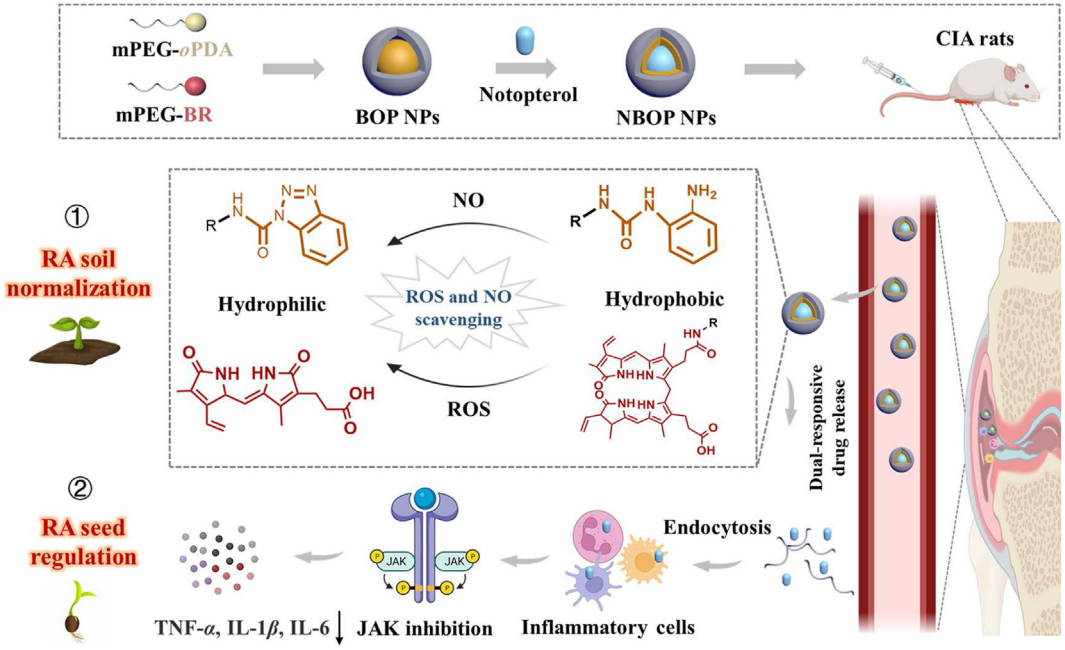

Scheme 1 Schematic illustration of the fabrication process of Not@BR/*o*PDA-PEG (NBOP) nanoparticles and the therapeutic mechanism based on regulating RA soils (ROS and NO scavenging) and seeds (JAK-STAT downregulation).

ELISA kits were bought from NeoBioscience Technology Co., Ltd. (Shenzhen, China). 3-(4,5-Dimethylthiazol-2-yl)-2,5-diphenyltetrazolium bromide (MTT), Dulbecco's modified Eagle's medium (DMEM), penicillin-streptomycin, fetal bovine serum (FBS), and trypsin with EDTA were purchased from Thermo Fisher (MA, USA). RAW264.7 cells were purchased from ATCC (Virginia, USA) and cultured in DMEM medium containing 10% FBS and 1% antibiotics (penicillin and streptomycin) at 37 °C and 5% CO_2. Female BALB/c mice (7 weeks, 20 ± 5 g) were purchased from Guangdong medical laboratory animal center (Guangzhou, China). Male Wistar rats (7 weeks, 200−300 g) were purchased from Charles River (Beijing, China). All animal experiments were performed under the guidelines evaluated and approved by the Experimental Animal Ethics Committee of the Zhuhai campus of the Zunyi Medical University.

2.2. *Synthesis of BR-PEG*

The synthetic method of BR-PEG was modified from the literature[20]. Bilirubin (BR, 1.49 mg, 2.5 μmol/L) was dissolved in 1 mL of chloroform, 1-(3-dimethylaminopropyl)-3-ethylcarbodiimide hydrochloride (EDC·HCl, 1.46 mg) and *N*-hydroxysuccinimide (NHS, 0.88 mg) were both dissolved in 1 mL of chloroform, added to the round-bottom flask in sequence and stirred for 1 h in the dark to activate carboxyl. Then $mPEG_{2000}$-NH_2 (12.5 mg, 2.5 μmol/L) was dissolved in 1 mL of chloroform and mixed with the BR solution. The mixture was stirred at room temperature in the dark for 12 h, washed three times with 0.1 mol/L HCl, and the organic phase was collected. Chloroform was removed by rotary evaporation, and then the product was dissolved in methanol and the precipitate was removed by filtration. The product after rotary evaporation was dissolved in chloroform and stored until use. Infrared (Thermo Fisher Scientific, Nicolet iS10, Waltham, MA, USA) and ^{1}H NMR spectrogram (Bruker, Ascend 600, Billerica, MA, USA) were used to characterize the product.

2.3. *Synthesis of APUEMA*

2-[3-(2-Aminophenyl)ureido]ethyl methacrylate (APUEMA) monomer was synthesized for further fabrication of PEGylated *o*-phenylenediamine (*o*PDA) through the method in the reported literature[21]. Briefly, *o*-phenylenediamine (2.7 g, 25 mmol) was dissolved in 100 mL of anhydrous acetonitrile. Isocyanoethyl 2-methacrylate (3.88 g, 25 mmol) was dissolved in 20 mL of anhydrous acetonitrile and added dropwise to the *o*-phenylenediamine-containing acetonitrile solution. The mixture was stirred at room temperature overnight. The acetonitrile was removed by rotary evaporation and the residue was precipitated into excess diethyl ether to remove any unreacted *o*-phenylenediamine and isocyanoethyl 2-methacrylate. The insoluble solid was collected and washed 3 times with ether. APUEMA was obtained as a white solid.

2.4. *Synthesis of oPDA-PEG*

*o*PDA-PEG was synthesized according to the synthetic method in the reported literature[22]. Briefly, 10 mg of APUEMA was dissolved in 2 mL of tetrahydrofuran, 111 mg of $mPEG_{2000}$-SH was dissolved in 3 mL of tetrahydrofuran, and 4 mg of benzoin dimethyl ether was dissolved in 1 mL of tetrahydrofuran as the click reaction catalyst. They were added to the round-bottomed flask in sequence and stirred. The tetrahydrofuran solution was irradiated with ultraviolet light with a light power of 100 mW/cm^2 and sealed in the dark. After 2 h, most of the tetrahydrofuran was removed by rotary evaporation. Excess ether was added to the remaining tetrahydrofuran solution to mix and centrifuge at 2000 rpm for 3 min (Thermo Fisher Scientific, Heraeus multifuge

X3R, Waltham, MA, USA). The supernatant was discarded, and the procedure was repeated twice. The precipitate was vacuum-dried down in a vacuum desiccator for 12 h at 30 °C to obtain *o*PDA-PEG. IR and ^{1}H NMR spectrogram were used to characterize *o*PDA-PEG.

2.5. Preparation of Not@BR/oPDA-PEG (NBOP) nanoparticles

The synthesis method of NBOP nanoparticles was modified from the literature[23]. BR-PEG and *o*PDA-PEG were prepared into a 10 mg/mL solution in chloroform for use. The ratios of BR-PEG and *o*PDA-PEG were mixed in a ratio of 1:2 (*m*/*m*), 1:1 (*m*/*m*), and 2:1 (*m*/*m*), respectively, and the total weight was 6 mg. Notopterol (Not) chloroform solution (10 mg/mL, 100 μL) was added and then supplemented by 7 mL of deionized water, which was emulsified with an ultrasonic homogenizer (Bilon, 250Y, Shanghai, China), the operating parameters are ultrasonic 5 s, interval 5 s, total time 5 min, 40 W. The mixture was fragmented by sonication in ice bath. Chloroform was removed by rotary evaporation to obtain NBOP nanoparticles with different BR-PEG/*o*PDA-PEG ratios. NBOP nanoparticles were stored at 4 °C in the dark for further use. Not@BR-PEG (NBP) nanoparticles and Not@*o*PDA-PEG (NOP) nanoparticles were fabricated *via* the same method.

2.6. Characterization of NBOP nanoparticles

The particle size, zeta potential and the stability of NBOP nanoparticles with different BR-PEG/*o*PDA-PEG ratios were measured by Zetasizer (Nano-ZS90, Malvern Panalytical, Malvern, Worcestershire, UK) based on dynamic light scattering (DLS) method to screen the appropriate ratio of BR/*o*PDA-PEG. The morphology of NBOP nanoparticles was observed by scanning electron microscope (SEM, Zeiss Merlin Gemini, Taufkirchen, Germany). The UV−Vis−NIR spectra of Not, BR-PEG, *o*PDA-PEG and NBOP nanoparticles were obtained by spectrophotometer (U-4100, Hitachi, Tokyo, Japan).

2.7. Encapsulation efficiency and drug loading of NBOP nanoparticles

The concentration of Not was determined by high performance liquid chromatography (HPLC) using a ZORBAX Eclipse Plus C18 Column (5 μm, 4.6 mm × 150 mm, Waters) with an injection volume of 10 μL and a detection wavelength of 310 nm at 30 °C. The mobile phase was water and acetonitrile with 0.1% formic acid by gradient elution at pre-determined ratios (*v*/*v*), from 65: 35 to 5: 95 (0−8 min), 5: 95 to 65: 35 (8−10 min), 65: 35 (10−12 min) with the flow rate of 1 mL/min. A standard curve could be obtained by performing linear regression processing on the absorbance values corresponding to each concentration. The encapsulation efficiency of drug Not was determined by the ultrafiltration method. Specifically, 1 mL of NBOP aqueous solution was added to the filter layer of an Amicon® Ultra-4 ultrafiltration tube (MWCO 10 k Da), and centrifuged at 4000 rpm for 20 min (Thermo Fisher Scientific, Heraeus multifuge X3R, Waltham, MA, USA). The unencapsulated drug was centrifuged to the bottom of the ultrafiltration tube. The aqueous solution containing the unencapsulated drug and the aqueous solution of NBOP nanoparticles were diluted with methanol and demulsified by ultrasonic. The drug content was detected by HPLC (Waters, e2695, Milford MA, USA). According to the standard curve, the concentration of Not in the solution was calculated, and then the drug loading and encapsulation efficiency of NBOP nanoparticles was evaluated as Eqs. (1) and (2), which were also used to determine the BR/*o*PDA-PEG ratio.

$$\text{Encapsulation efficiency (EE, \%)} = (\text{The amount of total drug} - \text{The amount of unencapsulated drug}) / (\text{The amount of total drug}) \times 100 \quad (1)$$

$$\text{Drug loading (DL, \%)} = \text{The amount of drug in the nanoparticle} / (\text{The amount of initially added drug} + \text{The amount of the initially added polymer}) \times 100 \quad (2)$$

2.8. In vitro drug release

NBOP nanoparticles were dialyzed against PBS (pH 7.4), H_2O_2/PBS (1 mmol/L H_2O_2), NO/PBS (0.1 mmol/L NO) and H_2O_2/NO/PBS containing Tween 20 (1%, *w*/*w*) at 37 °C 1 mL of medium was taken out in each sample at 1, 2, 4, 8, 12, 24, 48 and 72 h, while 1 mL of fresh medium was added. NO concentration in the samples was measured by HPLC.

2.9. Cytotoxicity of NBOP nanoparticles

The cytotoxicity of NBOP nanoparticles was evaluated using the MTT assay. RAW264.7 cells were seeded in 96-well plates at a density of 1×10^4 cells/well, and incubated with or without LPS for 48 h. Different concentrations of NBOP nanoparticles were added to each well, and incubated at 37 °C for 24 h. Then, the medium was replaced by 100 μL of MTT solution (1 mg/mL) for 4 h incubation at 37 °C 100 μL of DMSO was added to each well to shake for 10 min to dissolve the formazan crystals produced by living cells. The 96-well plate was placed in a microplate reader (Molecular Devices, SpectraMax M5, Silicon Valley, CA, USA), and the absorbance value of each well was measured at 490 nm. Cell viability (%) was calculated as Eq. (3):

$$\text{Cell viability (\%)} = A_{\text{treated}}/A_{\text{control}} \times 100 \quad (3)$$

where A_{treated} and A_{control} represented the absorbance of cells treated with different formulations and control group, respectively.

2.10. Cellular uptake of NBOP nanoparticles

The uptake of nanoparticles by LPS-stimulated Raw 264.7 cells was qualitatively investigated by an inverted fluorescence microscope and quantified by flow cytometry. RAW264.7 cells seeded in 24-well plate (5×10^4 cells per well) were treated for 24 h with or without LPS (10 μg/mL). Then cells were incubated with coumarin-6-labeled BOP nanoparticles (0.25 μg/mL) for 4 h and washed with PBS three times. Nuclei were stained with Hoechst 33,342 (1 μg/mL), followed by washing three times with PBS. The cells were imaged by an inverted fluorescence microscope (Leica, DMI8, Wetzlar, Germany). The fluorescence intensity was quantified by flow cytometry (Beckman Coulter, CytoFLEX, Brea, CA, USA).

2.11. Intracellular ROS scavenging

RAW264.7 cells were seeded in a 24-well plate at a density of 5×10^4 per well, and LPS (10 μg/mL) was added to stimulate for

24 h. After the cells were treated with NBP (20 μmol/L), NOP (20 μmol/L) and NBOP nanoparticles (20 μmol/L) for 24 h, cells were treated with DCFH-DA (5 μmol/L) and observed by fluorescence microscope (Leica). Flow cytometry analysis was performed to quantify the DCFH-DA fluorescence intensity of the cells. The hydrogen peroxide level in culture supernatant was evaluated by employing a hydrogen peroxide assay kit.

2.12. Intracellular NO scavenging

RAW 264.7 cells (5×10^4 cells/well) were seeded and stimulated by LPS (10 μg/mL) for 24 h while cells without LPS stimulation were used as the control. The cells were treated with NBP (20 μmol/L), NOP (20 μmol/L) and NBOP nanoparticles (20 μmol/L) for 24 h and then treated with NO probe DAF-FM-DA. The cells were observed by DMI8 fluorescence microscope (Leica). Flow cytometry analysis was performed to quantify the fluorescence intensity of the cells. Nitric oxide levels in cell supernatant of different groups were detected by a Griess assay kit.

2.13. Pharmacokinetic study in vivo

The pharmacokinetic experiments were investigated in mice as follows: 1. Free Not; 2. NBOP nanoparticles. The injection dose of Not was 5 mg/kg. Except for group 2 that was administered by intraperitoneal injection, the other groups were administered intravenously. Blood was collected at 30 min, 1, 2, 4, 6, 8, 12, and 24 h after administration. An appropriate amount of methanol was added to dissolve the drugs in the blood. The supernatant after centrifugation was collected for detection by HPLC (Waters).

2.14. CIA rat model

Collagen-induced arthritis (CIA) model was established in Wistar rats according to the protocol of manufacture (Chondrex, Inc., NE Redmond, WA). 2 mg/mL bovine type II collagen was emulsified with an equal volume of incomplete Freund's adjuvant (IFA) to prepare a CII emulsion with a final concentration of 1 mg/mL. Except for the control group, the rats of other groups were intradermally injected with CII emulsion (200 μL/rat) at the tail root, as the primary immunization. After 21 days, a booster immunization was performed with a similar method at the same concentration of CII emulsion.

2.15. Biodistribution of NBOP in CIA and normal rats

Normal and CIA rats received an intravenous injection of DiR-labeled NBOP. In addition, CIA model rats were also injected with free DiR intravenously. Rats were anesthetized without skin removal, and the distribution of nanoparticles was imaged using an *in vivo* fluorescence imaging system (IVIS, PerkinElmer, Waltham, MA, USA) before administration and 1, 3, 6, and 24 h after administration. The fluorescence intensity was analyzed using the Living Image software (PerkinElmer).

2.16. In vivo therapeutic efficacy of NBOP nanoparticles

The CIA model rats were randomly divided into six groups and treated with PBS, BP nanoparticles, OP nanoparticles, BOP nanoparticles, free Not and NBOP nanoparticles every three days, respectively. Most groups were intravenously injected except for the group of free Not using intraperitoneal injection. The dose was 5 mg/kg for notopterol and/or 15 mg/kg for BR-PEG/*o*PDA-PEG. Throughout the therapy, arthritis scores (0−4) were examined according to the standard rule every three days: 0, normal; 1, mild erythema of ankle joints; 2, mild erythema and swelling extending from the ankle to the tarsals; 3, moderate erythema and swelling from ankle to metatarsal joints; 4, severe erythema and swelling of the entire paw. For each rat, the scores of four paws were summed to obtain the total/overall arthritic score (maximum scores = 16). The volume and thickness of the hind paw were also measured every three days. On Day 30, the hind paws of rats receiving different treatments were photographed to evaluate the therapy outcome.

2.17. Micro-CT analysis

After anesthetized rats, local micro-CT scans were performed on the hind limbs of rats with microPET/CT (Mediso, nanoScan PET/CT 82s, Budapest, Hungarian). The obtained data were processed to form the 3D structure of joint.

2.18. In vivo ROS and NO scavenging effect of NBOP nanoparticles

The *in vivo* ROS and NO scavenging effect of NBOP nanoparticles were evaluated in CIA rat model as the literature reported[24]. The serum of different treatment groups was collected at 24 h after injecting PBS, BP nanoparticles, OP nanoparticles, BOP nanoparticles, free Not and NBOP nanoparticles to evaluate the levels of H_2O_2 and NO in serum through using the hydrogen peroxide assay kit and nitric oxide assay kit, respectively.

2.19. Histopathologic evaluation

After all rats were sacrificed, the collected ankle joints were fixed and decalcified for 45 days. The samples were embedded and sliced to perform hematoxylin and eosin (H&E), safranin O, and toluidine blue (TB) staining. Immunohistochemical staining (JAK2, STAT3, STAT5) and immunofluorescence staining (iNOS, CD206) were also performed as described in the literature[25], to verify the JAK-STAT inhibition effect and M1-to-M2 polarization capacity of NBOP nanoparticles.

2.20. In vivo cytokine evaluation

After all rats were sacrificed, the collected whole blood of CIA rat was allowed to clot at 37 °C for 1 h, followed by centrifugation at 3500 rpm for 10 min (Thermo Fisher Scientific, Sorvall legend micro 21 R, Waltham, MA, USA). The serum samples were collected from the supernatant to measure the levels of TNF-α, IL-6, IL-1β by using rat TNF-α, IL-6, IL-1β ELISA kits.

2.21. Biosafety evaluation

The body weight of CIA rats was recorded during the treatments. After sacrificing the rats, major organs (heart, liver, spleen, lung, and kidney) were collected and fixed with 4% paraformaldehyde to perform H&E staining.

2.22. Statistical analysis

All experiments were performed three times and all data were presented as mean with standard deviation (SD). Statistical

significance was calculated by Student's *t*-tests and one-way ANOVA using GraphPad Prism 7 (San Diego, CA, USA). $^{*}P < 0.05$, $^{**}P < 0.01$, $^{***}P < 0.001$ were considered a significant difference.

3. Results and discussion

3.1. Synthesis of BR-PEG and oPDA-PEG

PEGylated bilirubin (BR-PEG) was synthesized through conjugating hydrophobic bilirubin to hydrophilic PEG molecules *via* the amide bond (Supporting Information Fig. S1). As shown in Supporting Information Fig. S2, characteristic absorption bands derived from bilirubin and PEG-NH_2 could be observed in the infrared spectrum of BR-PEG, such as the band at 1700−1600 cm^{-1} of bilirubin, and the stretching due to the hydroxyl group 3410 cm^{-1} absorption peak produced by vibration. Characteristic peaks from PEG-NH_2 at 2888 and 1112 cm^{-1} were also observed, proving that BR-PEG was successfully synthesized. BR-PEG had the characteristic chemical shift peak of its reactant (bilirubin and mPEG-NH_2) in ^{1}H NMR spectra, which confirmed the structure of BR-PEG (Supporting Information Fig. S3). 2-[3-(2-Aminophenyl)ureido]ethyl methacrylate (APUEMA) monomer, a novel nitric oxide (NO) responsive monomer containing *o*-phenylenediamine (*o*PDA) functional groups were fabricated to be conjugated to thiol PEG (PEG-SH) to obtain *o*PDA-PEG *via* click reaction. The successful synthesis of *o*PDA-PEG has been demonstrated by IR spectroscopy and ^{1}H NMR spectroscopy (Supporting Information Figs. S4 and S5). Specifically, characteristic absorption bands derived from APUEMA and mPEG-SH could be observed in the IR spectrum of *o*PDA-PEG, such as the band at 1750−1500 cm^{-1} of APUEMA, and the 3311 cm^{-1} absorption peak produced by the stretching vibration of the amide. At the same time, a characteristic peak from mPEG-SH at 2887 cm^{-1} was also observed. *o*PDA-PEG also contained characteristic peaks of APUEMA and mPEG-SH in ^{1}H NMR.

3.2. Preparation and characterization of NBOP nanoparticles

Amphiphilic PEGylated bilirubin and PEGylated *o*-phenylenediamine could self-assemble to form nanoparticles due to the hydrophobic interaction. The hydrodynamic diameters of Not@BR/*o*PDA-PEG (NBOP) with 1/2, 1/1, and 2/1, and BR-PEG/*o*PDA-PEG ratios were 289.0 ± 158.6, 137.7 ± 2.1, 177.4 ± 16.8 nm, respectively (Fig. 1A). NBOP at the feeding ratio (1/1 BR-PEG/*o*PDA-PEG) was optimal with uniform particle size and decent encapsulation efficiencies, which was used in the following experiments. The prepared NBOP nanoparticles possessed the average diameter of 137.7 nm (Fig. 1B) with a little positive potential of +4.69 mV, and had the largest drug loading efficiency of 9.53% and encapsulation efficiency of 91.01%. Scanning electron microscopy (SEM) image of NBOP nanoparticles showed monodispersed spherical nanoparticles with a diameter of approximately 140 nm (Fig. 1C), which was consistent with the results measured using dynamic light scattering (DLS). The size of NBOP nanoparticles was suitable for drug delivery to treat RA *via* extravasation through leaky vasculature and subsequent inflammatory cell-mediated sequestration (ELVIS) effect. UV−Vis spectroscopy was performed to further confirm the fabrication of NBOP nanoparticles. NBOP nanoparticles and Not exhibited a maximum absorption peak at around 310 nm, compared with no obvious absorbance for BR-PEG and *o*PDA-PEG (Fig. 1E). The long-term stability of NBOP nanoparticles was also investigated. The size and PDI of NBOP nanoparticles stored at 4 °C did not show a significant change for 7 days, suggesting the good stability of the NBOP nanoparticles (Fig. 1D and Supporting Information Fig. S6). The *in vitro* release profiles of Not from NBOP were

A

BR-PEG: *o*PDA-PEG	Size (nm)	PDI	Potential (mV)	EE (%)	DL (%)
1:2	289.0±158.6	0.326±0.102	9.2±1.2	88.73	2.79
1:1	137.7±2.1	0.223±0.031	4.7±1.0	91.01	9.53
2:1	177.4±16.8	0.259±0.023	15.1±3.3	80.20	8.77

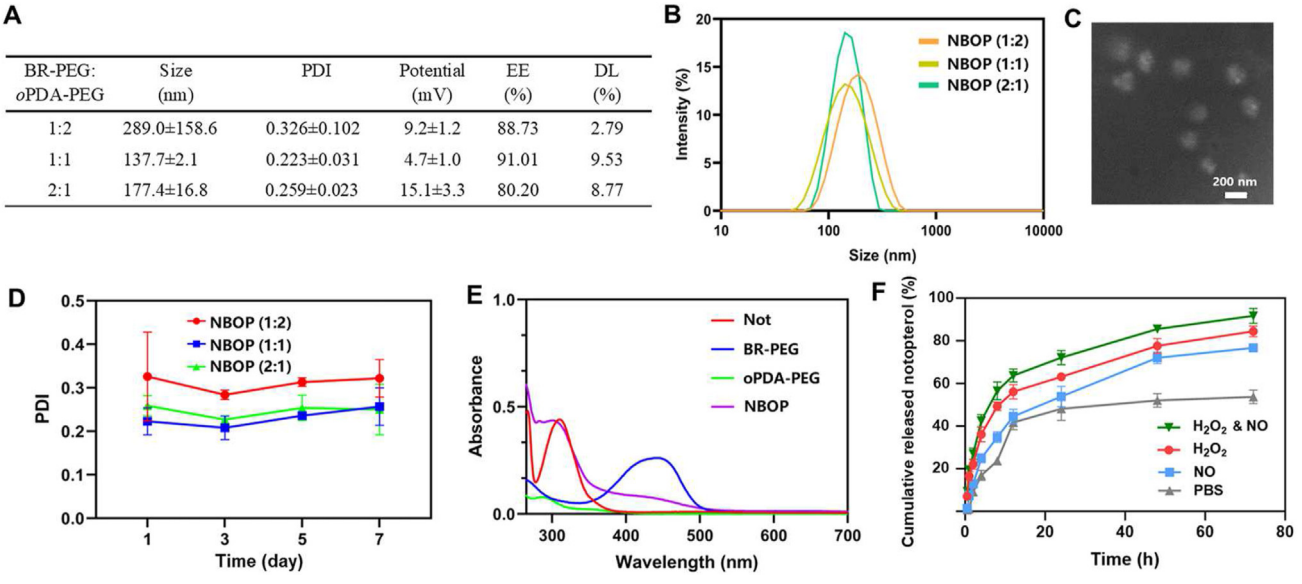

Figure 1 Physicochemical characterization of NBOP nanoparticles. (A) Particle size, PDI, potential, encapsulation efficiency and drug loading of NBOP at three ratios. (B) Particle size distribution, (C) SEM image, (D) stability test and (E) UV absorption spectrum of Not (100 μg/mL), BR-PEG (1 mg/mL), oPDA-PEG (1 mg/mL) and NBOP nanoparticles loaded with Not (100 μg/mL). (F) Drug release profiles of NBOP nanoparticles containing H_2O_2 (1 mmol/L) and/or NO (100 μmol/L) *in vitro*. Data are shown as mean ± SD ($n = 3$).

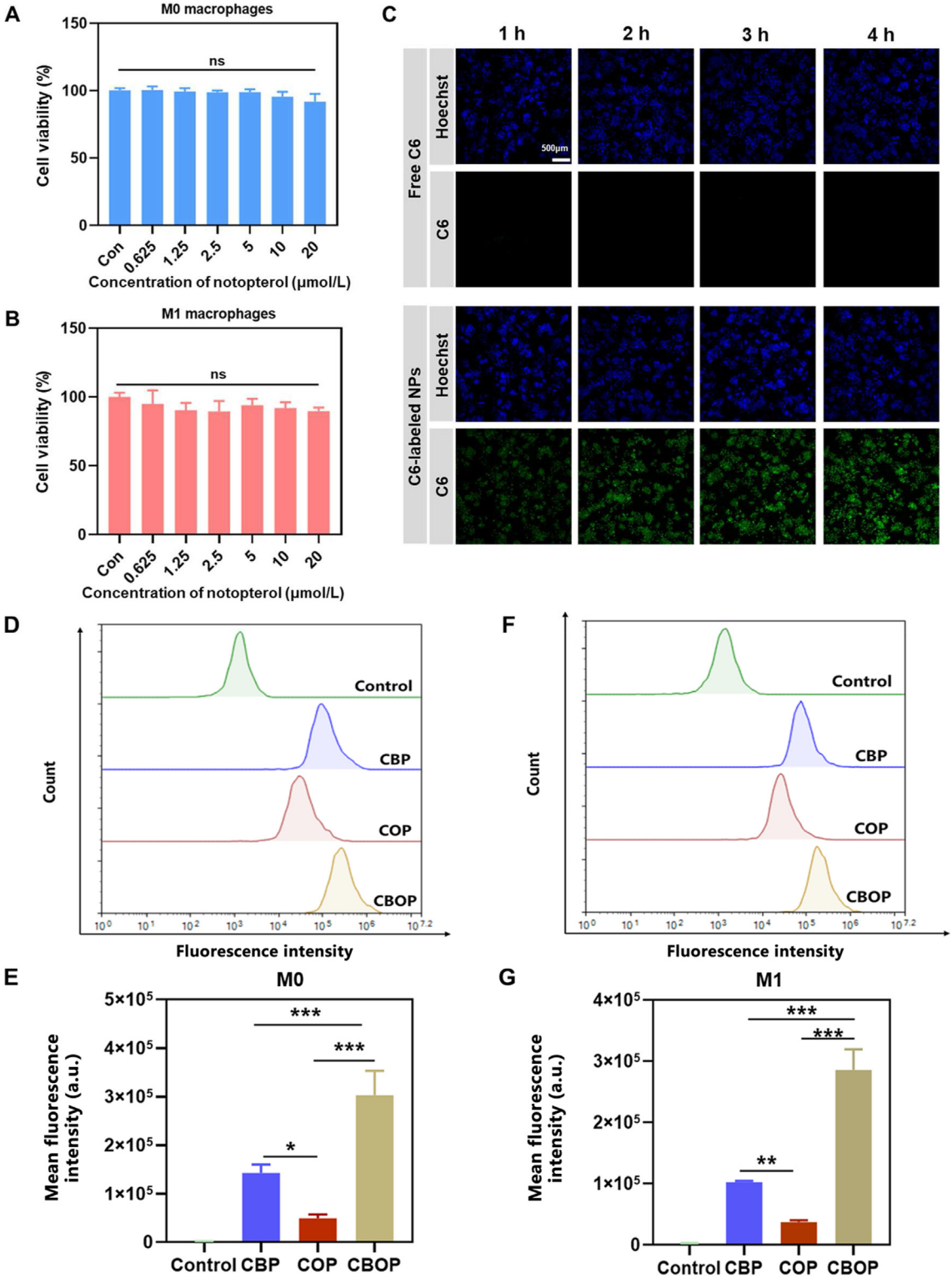

Figure 2 Cytotoxicity and uptake of NBOP nanoparticles. Cell viability of NBOP NPs in (A) M0 and (B) M1 cells. (C) Cellular uptake of free C6 and C6-labeled BOP nanoparticles in RAW264.7 cells pictured by fluorescent microscope. Scale bar = 500 μm. Flow cytometry analysis of cellular uptake of CBP, COP and CBOP NPs in (D) M0 macrophages and (F) M1 macrophages. Quantitative analysis of the fluorescence intensity of CBP, COP, and CBOP NPs in (E) M0 macrophages and (G) M1 macrophages. Data are shown as mean ± SD ($n = 3$), $^{*}P < 0.05$, $^{**}P < 0.01$, $^{***}P < 0.001$ *vs*. indicated, ns, no significant difference in comparison with the control group.

investigated by the dialysis method. Only 54% of Not was released in the absence of H_2O_2 and NO. However, around 85% and 77% of total Not were released from NBOP nanoparticles after treatment of 1 mmol/L H_2O_2 and 100 μmol/L NO for 72 h, respectively (Fig. 1F). These results indicated that NBOP nanoparticles exhibited dually ROS and NO responsive drug release

due to the ROS-responsive moiety bilirubin and NO responsive moiety *o*-phenylenediamine promoting NBOP disintegration in the presence of H_2O_2 and NO.

3.3. *Cytotoxicity and uptake of NBOP nanoparticles*

MTT assay was performed to evaluate the biosafety of NBOP nanoparticles to M0 and M1 macrophages. RAW264.7 cells were pretreated with lipopolysaccharide (LPS) to allow M1 polarization to investigate the cytotoxicity of NBOP nanoparticles to M1 macrophages. As shown in Fig. 2A and B, no toxicity of NBOP nanoparticles was observed at the Not equivalent concentration range (0.625−20 μmol/L) in both M0 and M1 macrophages. It is worth noting that free Not at a concentration of 20 μmol/L showed strong toxicity when exposed to cells (Supporting Information Fig. S7). The toxicity of Not and NBOP to MH7A cells was similar to that of RAW264.7 cells (Supporting Information Fig. S8). These results indicated that bilirubin and *o*-phenylenediamine modification did not affect the biocompatibility of polyethylene glycol, and Not was safe for further use at a dose below 20 μmol/L. Macrophages are regarded as the most crucial roles in RA by generating pro-inflammatory cytokines to exacerbate inflammation. Thus, we next explored the cellular uptake of NBOP nanoparticles. Coumarin 6 (C6) was loaded as model hydrophobic drug. C6@BR/*o*PDA-PEG (CBOP) nanoparticles exhibited much stronger green fluorescence compared with that of free C6 at 1, 2, 3 and 4 h, demonstrating that the encapsulation by BOP could significantly improve the cellular uptake (Fig. 2C). Interestingly, the uptake of CBOP nanoparticles by M0 macrophages was 2.1 times higher than that of C6@BR-PEG (CBP) nanoparticles and 6.2 times higher than that of C6@*o*PDA-PEG (COP) nanoparticles (Fig. 2D and E). Bilirubin modification significantly enhanced the cellular uptake efficiency, which might be attributed to the bilirubin receptor expressed in macrophages[26,27]. Similar cellular uptake results were also observed in M1 macrophages (Fig. 2F and G). These results confirmed that NBOP nanoparticles could effectively target macrophages *in vitro*.

3.4. *Intracellular ROS scavenging capability of NBOP nanoparticles*

2',7'-Dichlorodihydrofluorescein diacetate (DCFH-DA) was employed to quantify the overall oxidative stress in cells for evaluating the intracellular ROS depletion capacity of NBOP. LPS-stimulated macrophages (M1) showed a significantly brighter DCFH-DA fluorescence emission than M0 macrophages (Fig. 3A). Not@*o*PDA-PEG (NOP) nanoparticles did not influence the ROS level. However, Not@BR-PEG (NBP) nanoparticles and NBOP nanoparticles both significantly reduced the green fluorescence, indicating an effective ROS depletion activity of bilirubin modification nanoparticles. The intracellular DCFH-DA signal was further quantified by flow cytometry (Fig. 3B). The fluorescence intensity of DCFH-DA in NBP and NBOP group decreased to about 39% and 64% compared with that in the LPS-stimulated macrophages, which was consistent with the fluorescence imaging result (Fig. 3D). In addition, we evaluated the hydrogen peroxide level of the culture supernatant in the different nanoparticle-treated group by using hydroperoxide assay with the ferric−xylenol orange complex. The hydrogen peroxide level of the NBP and NBOP group was reduced by 30.6% and 14.4% compared with that of the

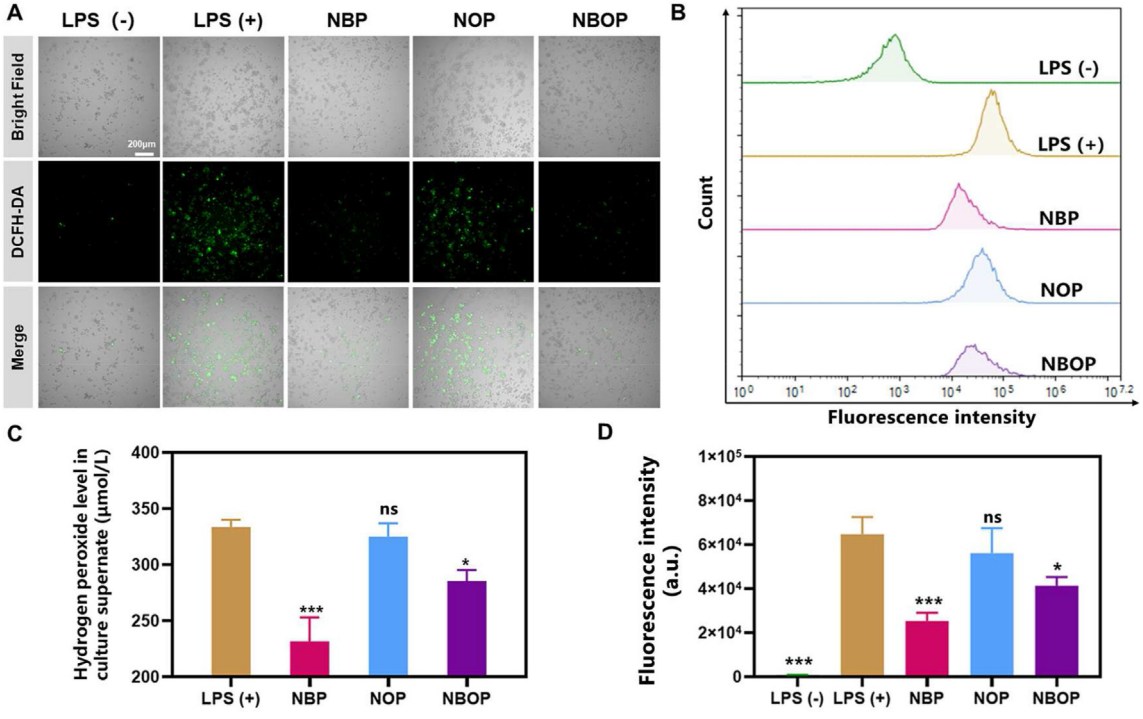

Figure 3 Intracellular ROS scavenging effect of NBOP nanoparticles. (A) Fluorescence imaging of the intracellular ROS treated by NBP (20 μmol/L), NOP (20 μmol/L) and NBOP NPs (20 μmol/L) using DCFH-DA (green) probe. Scale bar = 200 μm. (B) Flow cytometry analysis of intracellular ROS level. (C) Hydrogen peroxide level in culture supernatant treated by NBP, NOP and NBOP NPs. (D) Quantitative analysis of DCFH-DA intensity. Data are shown as mean ± SD. ($n = 3$). *$P < 0.05$, ***$P < 0.001$ *vs.* indicated, ns, no significant difference in a comparison with LPS (+) group.

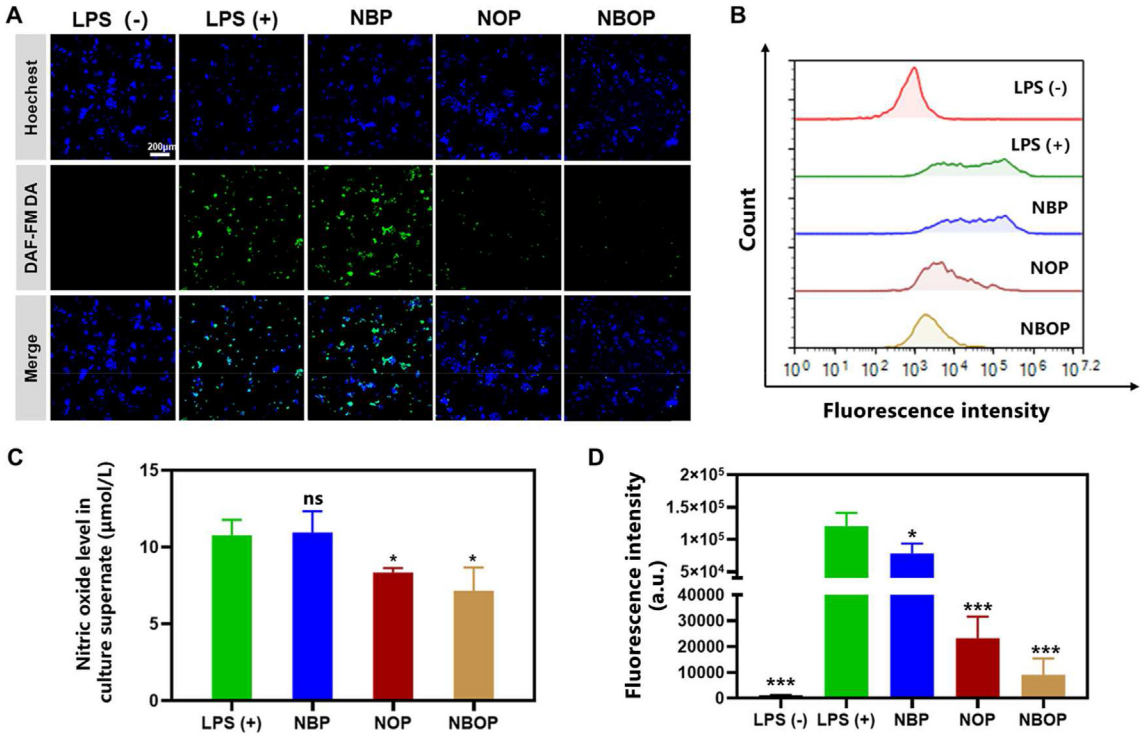

Figure 4 Intracellular nitric oxide depletion effect of NBOP nanoparticles. (A) Fluorescence imaging of the intracellular NO treated by NBP (20 μmol/L), NOP (20 μmol/L) and NBOP NPs (20 μmol/L) using DAF-FM DA (green) probe. Scale bar: 200 μm. (B) Flow cytometry analysis of intracellular NO level. (C) NO level in culture supernatant treated by NBP, NOP and NBOP NPs. (D) Quantitative analysis of DAF-FM DA intensity. Data are shown as mean ± SD ($n = 3$). $^*P < 0.05$, $^{***}P < 0.001$, *vs.* indicated, ns, no significant difference in a comparison with LPS (+) group.

blank group in LPS-stimulated macrophages (Fig. 3C). These results revealed NBOP nanoparticles were promising candidates to relieve oxidative stress for RA therapy.

3.5. *Intracellular NO scavenging capability of NBOP nanoparticles*

Diaminofluorescein-FM diacetate (DAF-FM DA), a cell permeable fluorescent probe to detect intracellular NO was used to investigate the intracellular NO scavenging ability of NBOP. As shown in Fig. 4A, the DAF-FM DA signal was brighter in M1 macrophages than in the M0 macrophages. The fluorescence intensity was significantly reduced after treatment of NOP and NBOP nanoparticles, while NBP nanoparticles did not attenuate green fluorescence. Flow cytometry was used to quantify intracellular DAF-FM DA signal (Fig. 4B and D). The fluorescence intensity of DA-FM DA in M1 macrophages was significantly higher than that of M0, and the fluorescence intensity decreased by 4.2- and 12.3-fold after cells were treated with NOP and NBOP nanoparticles, respectively, indicating that the potent NO scavenging effect of

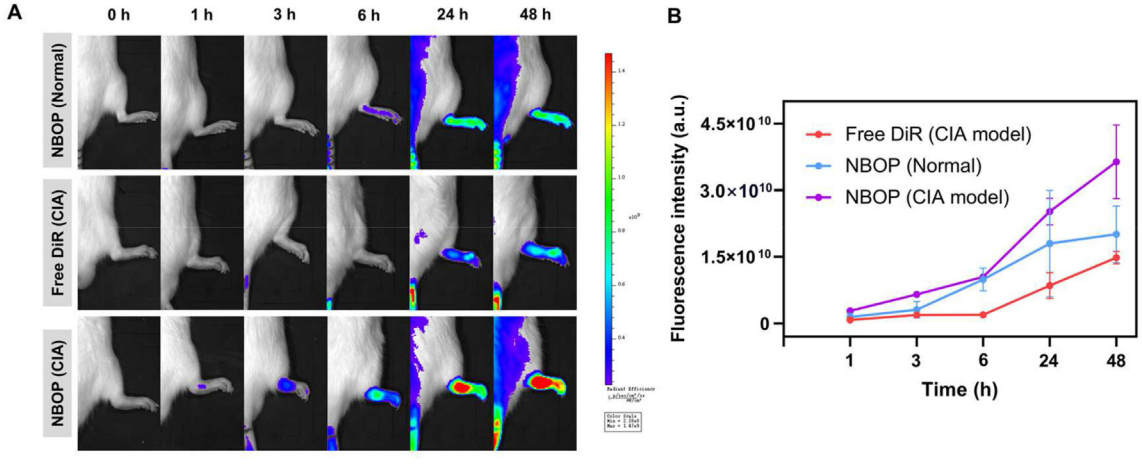

Figure 5 *In vivo* targeting of NBOP nanoparticles. (A) Fluorescence imaging of free DiR in CIA rats and DiR-labeled NBOP in normal and CIA rats at 0, 1, 3, 6, 24, and 48 h after intravenous injection. (B) Quantitative analysis of DiR intensity in (A). Data are shown as mean ± SD ($n = 3$).

NBOP nanoparticles. Moreover, the nitric oxide level in the culture supernatant was also evaluated by the Griess assay. NOP and NBOP also reduced the nitric oxide level in the culture supernatant, which was consistent with the DA-FM DA staining result (Fig. 4C). Hence, NBOP nanoparticles were effective in scavenging nitric oxide of macrophages for treating RA.

3.6. *Biodistribution of NBOP in vivo*

The free drug Not was injected intraperitoneally, and NBOP nanoparticles were injected intravenously into mice. The plasma concentration of the free drug was significantly lower than that of the NBOP group, and the area under the drug concentration−time curve (AUC) of the NBOP group was 2.8 times that of the free drug (Supporting Information Fig. S9). NBOP possessed a long circulation ability in blood and maintained a high drug concentration in the blood after 24 h of administration, which is beneficial to the drug delivery to the joint site to exert an anti-rheumatoid arthritis effect. To investigate the effect of the hind paw joint site on drug distribution in normal and CIA model rats, we evaluated whether NBOP nanoparticles in the CIA model possessed the targeting ability. NBOP nanoparticles were labeled with DiR, a near-infrared fluorophore, and injected intravenously into normal and CIA rats. Fluorescent signals could be observed in

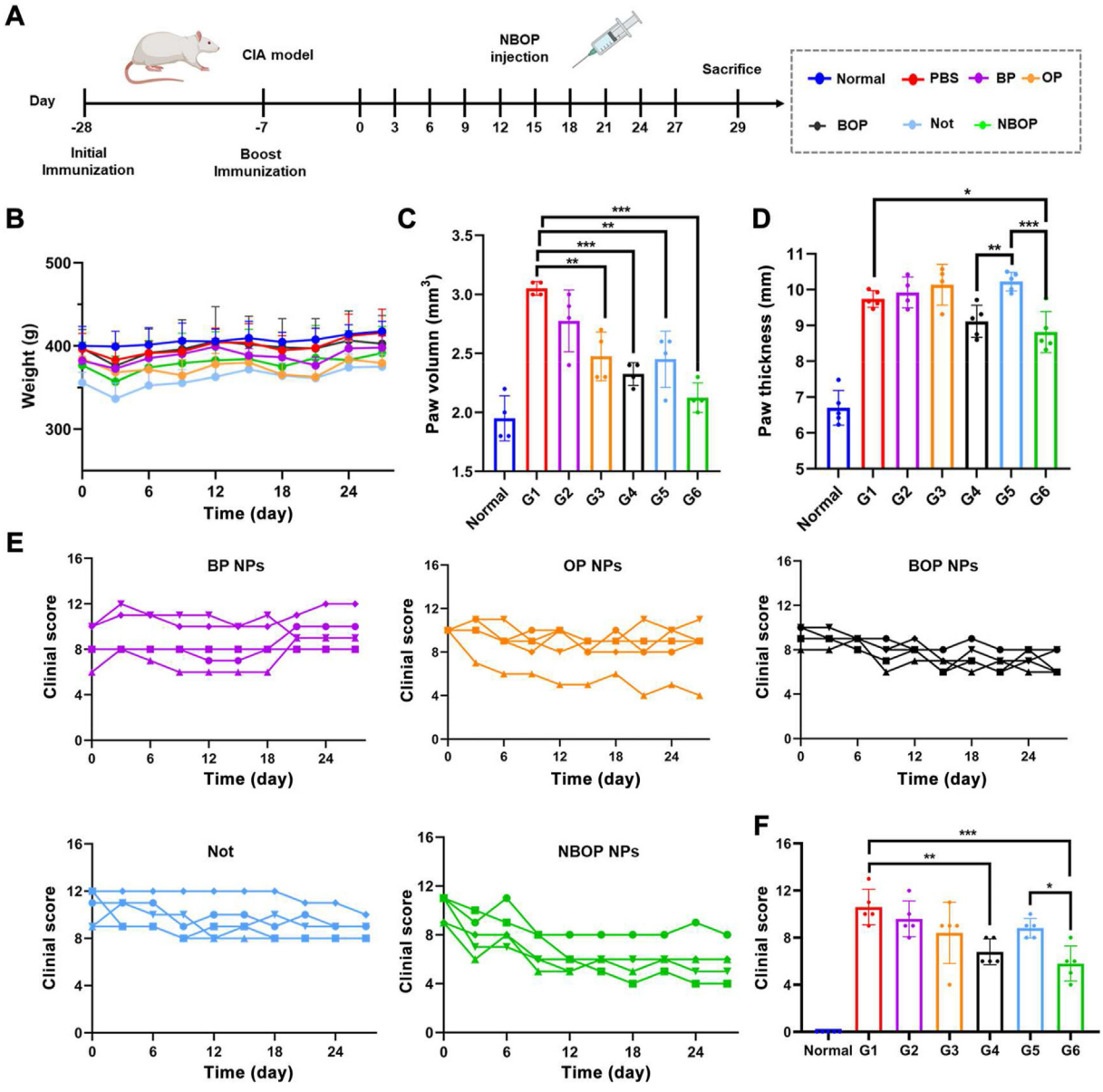

Figure 6 Therapeutic efficacy of NBOP nanoparticles. (A) Experimental outline for two immunizations and RA treatment. Rats received i.v. injection of PBS (1 × , G1), BP nanoparticles (15 mg/kg of BR-PEG, G2), OP nanoparticles (15 mg/kg of *o*PDA-PEG, G3), BOP nanoparticles (15 mg/kg of BR/*o*PDA-PEG, G4), NBOP nanoparticles (5 mg/kg of Not, G6), and i.p. injection of free Not (5 mg/kg, G5) every 3 days. (B) Weight changes of rats during treatment. (C) Paw volume of the rats in each treatment group at the end of the therapy. (D) Paw thickness of the rats in each treatment group at the end of the therapy. (E) Time-dependent clinical score for each rat in groups G2−G6. (F) Clinical scores of the rats in each treatment group at the end of the therapy. Data are presented as mean ± SD ($n = 5$). $^{*}P < 0.05$, $^{**}P < 0.01$, $^{***}P < 0.001$ *vs.* indicated.

the inflamed joints of CIA rats after 3 h post-injection and persisted for 48 h (Fig. 5A). In contrast, the fluorescent signal in the uninflamed joints of normal rats appeared only 6 h after injection. Notably, the mean flurencese intensity of the DiR@BOP group was significantly higher than that of the DiR@OP group at 48 h, which demonstrated the targeting ability after bilirubin modification (Supporting Information Fig. S10). In CIA rats, the area under the time-fluorescence intensity curve was 3-fold higher in the NBOP group than in the free DiR group (Fig. 5B). These results demonstrated that the NBOP group could target the inflamed joints of CIA rats, thereby enhancing drug delivery efficiency in the targeted tissues.

3.7. In vivo therapeutic effects of the NBOP treatment in the CIA model

The *in vivo* therapeutic efficacy of the NBOP nanoparticles was investigated on the CIA rat model as the treatment scheme outlined in Fig. 6A. Rats were randomly divided into 7 groups and administrated with PBS (referred to as G1), BP nanoparticles (G2), OP nanoparticles (G3), BOP nanoparticles (G4), free Not (G5) and NBOP nanoparticles (G6) twenty-eight days after the primary immunization. All treating groups didn't show obvious weight loss (Fig. 6B). The anti-RA efficacy was initially monitored by the hind paw volume, thickness, and clinical scores to reflect paw swelling extent in the CIA rats (Fig. 6C and D). Compared with severe swelling in the ankles and paws of the CIA rats treated by PBS, BP, OP and BOP nanoparticles exhibited a significant decrease in paw volume, demonstrating the drug-free nanocarriers could alleviate RA owing to the ROS and/or NO scavenging capacity. The paw volumes of rats in BOP group was obviously lower than those in BP and OP group, indicating the superior therapeutic potential of simultaneously scavenging ROS and NO. The free Not group just revealed the moderate suppressing swelling effect due to the poor joint accumulation and rapid clearance. Notably, the NBOP group showed the most obvious therapeutic efficacy in normalizing paw volume, which was attributed to the combinational effect of ROS and NO depletion mediated by the carrier and JAK-STAT inhibition functioned by Not. Similarly, the paw thickness in NBOP treated group was more significantly improved compared with the free Not group and BOP nanoparticle group (Fig. 6D). In addition, the clinical score is an important indicator to assess the anti-inflammatory effect during arthritis progression[28]. As shown in

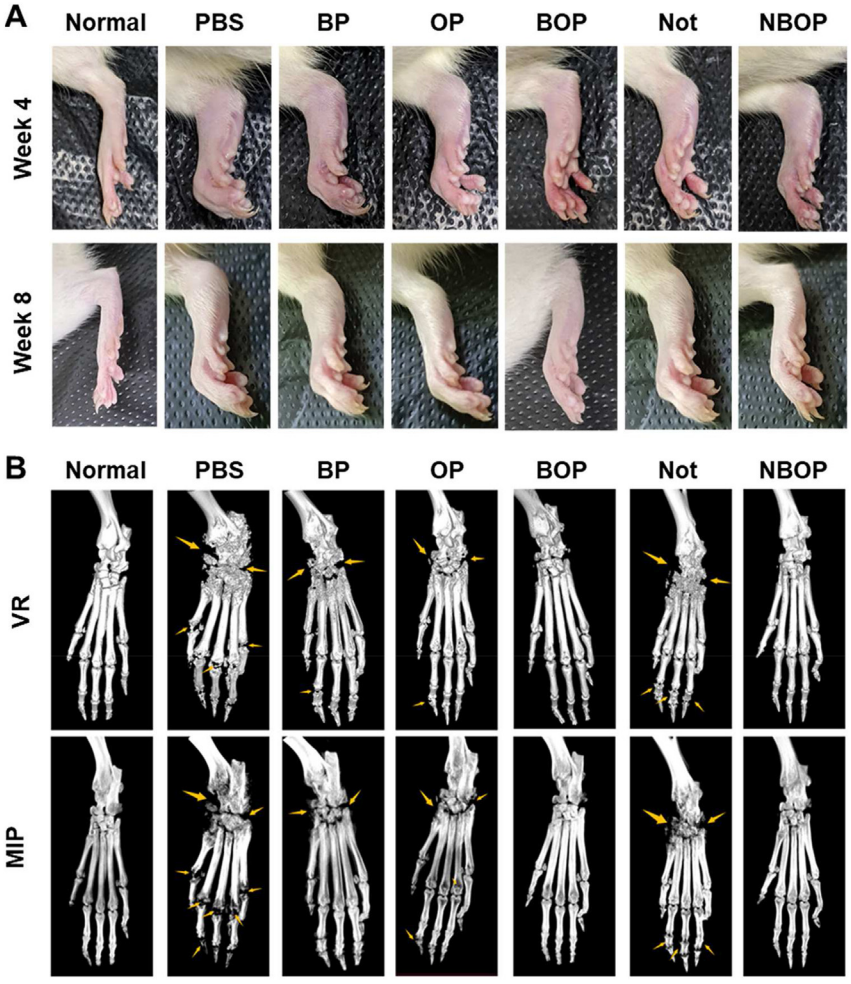

Figure 7 Representative images of the CIA rat model treated with NBOP nanoparticles. (A) Hind paw images of the treatment group at week 4 and week 8. (B) Micro-CT images of bone destruction in different groups. The yellow arrow indicated bone destruction and damage. The above row of images is processed using the volume rendering technique (VR), and the lower row of images is processed by the maximal intensity projection technique (MIP).

Fig. 6E, the arthritis clinical score rapidly increased in the PBS group, while the increase in clinical score was significantly lower in the free Not, OP nanoparticle, BOP nanoparticle and NBOP nanoparticle group. The clinical scores at the end of therapy for NBOP were the lowest, which was consistent with the result of paw volume and paw thickness (Fig. 6F). A similar therapeutic outcome was observed in the hind paw images (Fig. 7A). The anti-arthritis efficacy of NBOP nanoparticles was further evaluated *via* micro computed tomography (Micro-CT) imaging. After PBS treatment, rough bone surfaces and low bone mineral density were observed in the ankle and digits of rats due to severe bone erosion (Fig. 7B). After being treated with BP and OP groups, severe bone erosion in the ankle was slightly inhibited, which might be attributed to maintaining the mitochondrial structure and function of chondrocyte by scavenging ROS[29]. To be noted, excessive NO produced by RA in lesions could induce osteoclast upregulation, leading to bone resorption and chondrocyte apoptosis, and subsequently joint dysfunction[18,30,31]. A clear bone boundary with less bone erosion was observed in rats treated with OP and BOP nanoparticles, suggesting the therapeutic efficacy of NO scavenging to relieve bone erosions. Although the JAK inhibitor notopterol has been reported to decrease osteoclasts in synovial tissue for preventing bone erosions[19], severe bone resorption occurred in the ankle joint of rats treated with free drug Not as a result of the poor accumulation of free Not. In contrast, the ankle and digit bones of rats in NBOP groups had clear boundaries and few bone erosion as the normal group, indicating that NBOP nanoparticles were effective in bone protection for RA treatment.

We further confirmed the anti-arthritis efficacy by collecting the ankle joints of rats for histological examination at the study endpoint (Fig. 8A). H&E-stained sections of ankle joints from the saline group revealed severe synovial hyperplasia, extensive pannus formation, and obvious cartilage destruction. BP and OP group could partially reduce synovial inflammation and decrease cartilage destruction compared with the saline group. The BOP group revealed less extensive cartilage damage and pannus formation than BP or OP group. The free Not group exhibited a

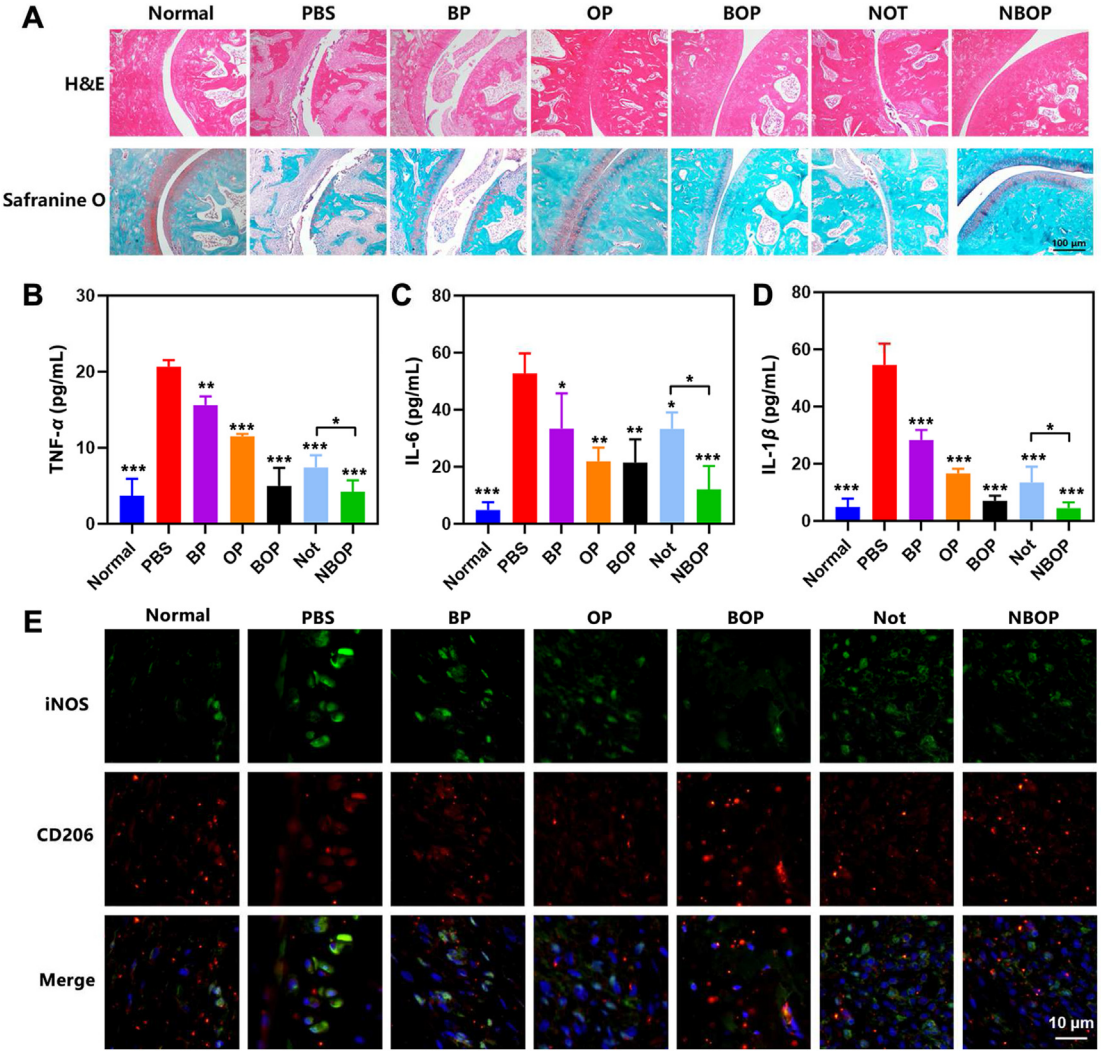

Figure 8 Histopathologic analyses and inflammation evaluations of CIA rat model treated with NBOP nanoparticles. (A) Histopathology images of ankle joints were evaluated by using H&E and safranin-O staining (scale bar = 100 μm). The serum concentration of pro-inflammatory cytokines includes (B) TNF-α, (C) IL-6, and (D) IL-1β. (E) The immunofluorescence staining of iNOS and CD206 for rat ankle joints after different treatments. Scale bar = 10 μm. Data are shown as mean ± SD. ($n = 3$). *$P < 0.05$, **$P < 0.01$, ***$P < 0.001$ in a comparison with PBS group.

restricted therapeutic efficacy in reversing these symptoms while the NBOP group showed the minimum pathologic features. The safranin O staining that stains glycosaminoglycans in cartilage exhibited a similar trend compared with H&E staining result. Severe cartilage damage was observed in the PBS group while BP and free Not groups didn't exert an obvious relieving cartilage damage effect. OP and BOP groups could effectively reduce cartilage damage owing to the NO scavenging effect. The cartilage seemed intact in rats treated with the NBOP group and the positive areas for safranin-O staining were closer to those of the normal group, which could be attributed to an effective combination of NO depletion and JAK-STAT inhibition. We have also evaluated the H_2O_2 and NO levels in the RA rat serum after 24 h of sample injection to reveal the *in vivo* ROS and NO scavenging capacity. The result in Supporting Information Fig. S11 exhibited that the level of H_2O_2 and NO in serum were significantly elevated in the CIA rat group compared with the healthy rat group. BOP and NBOP NPs could both decrease the H_2O_2 and NO to the normal level, in line with the *in vitro* ROS and NO scavenging results. The *in vivo* serum levels of proinflammatory cytokines (TNF-α, IL-6, IL-1β) were also measured after different treatments as another crucial index to evaluate therapeutic efficacy. BP, OP and BOP groups could significantly decrease the levels of TNF-α, IL-1β, and IL-6 without encapsulating other anti-inflammatory drugs, which verified the ROS and NO scavenging in relieving inflammation (Fig. 8B−D). Free Not showed moderate effect in lowering TNF-α, IL-1β, and IL-6 while the lowest levels of the cytokines were measured in rats treated with NBOP nanoparticles. In addition, ROS and NO scavenging could facilitate inflammatory M1 macrophage switching to the anti-inflammatory M2 phenotype[24,25,32]. Thus, we performed immunofluorescence staining of the M1 biomarker (iNOS) and M2 biomarker (CD206) to indirectly reveal the ROS and NO scavenging effect of NBOP *in vivo* (Fig. 8E). The macrophages rat ankle joints showed strong immunofluorescence signal of iNOS but weak signal of CD206 in PBS group. By contrast, a low iNOS signal and high CD206 signal could be observed with BOP and NBOP NPs, indicating successful M1 polarizing to M2. Moreover, the expression of JAK2, STAT3 and STAT5 was also investigated by immunohistochemical staining. Not and NBOP treatment induced lower expression levels of JAK2, STAT3 and STAT5 in inflamed joints compared with the PBS group while the BOP group didn't inhibit JAK2, STAT3 and STAT5 obviously (Supporting Information Fig. S12). No histopathological abnormalities or lesions after injecting different nanoparticles compared with those in the saline group, demonstrating the high biocompatibility of NBOP nanoparticles *in vivo* (Supporting Information Fig. S13). These results demonstrated that NBOP nanoparticles effectively relieved synovial inflammation and decreased joint damage to suppress RA progression *via* combining ROS/NO depletion and JAK-STAT inhibition.

4. Conclusions

Based on the purpose of inhibiting RA through regulating RA soils and seeds, we successfully synthesized BR-PEG, *o*PDA-PEG and NBOP nanoparticles for the delivery of notopterol. NBOP nanoparticles could specifically eliminate ROS and NO in the inflammatory microenvironment, resulting in the cleavage of nanoparticles and the release of the potent therapeutic drug notopterol. NBOP nanoparticles possessed uniform particle size distribution, weak positive charge, and good stability, which were suitable as a nano-drug delivery system for RA treatment. NBOP not only significantly increased the cellular uptake by macrophages, but also reduced ROS and NO levels of pro-inflammatory M1 phenotype. The *in vivo* experiments showed NBOP had significantly enhanced therapeutic efficacy compared to free notopterol and BOP. The anti-inflammatory mechanism of NBOP nanoparticles is related to scavenging ROS/NO and inhibiting the JAK-STAT signaling pathway. This study provided a reference for regulating RA soils and seeds for effective RA therapy.

Acknowledgments

This study was supported by the National Natural Science Foundation of China (51922111, 82204724), the Science and Technology Development Fund, Macau SAR (File no. 0124/2019/A3 and SKL-QRCM(UM)-2023-2025, China), and the University of Macau (File no. MYRG2022-00203-ICMS, China). We also appreciate the website of app.Biorender.com for assistance in preparing the scheme figure.

Author contributions

Peng Hua and Meiwan Chen designed the research. Hua Peng and Ruifeng Liang carried out the experiments and performed data analysis. Yanbei Tu and Yuying Yin participated in part of the experiments. Hua Peng and Ruifeng Liang wrote the manuscript. Man-Kay Law and Meiwan Chen revised the manuscript. All authors have read and approved the final manuscript.

Conflicts of interest

The authors declare no conflicts of interest.

Appendix A. Supporting information

Supporting data to this article can be found online at https://doi.org/10.1016/j.apsb.2023.07.021.

References

1. Lee DM, Weinblatt ME. Rheumatoid arthritis. *Lancet* 2001;**358**:903−11.
2. Scott DL, Wolfe F, Huizinga TW. Rheumatoid arthritis. *Lancet* 2010;**376**:1094−108.
3. Atzeni F, Rodríguez-Carrio J, Popa CD, Nurmohamed MT, Szűcs G, Szekanecz Z. Cardiovascular effects of approved drugs for rheumatoid arthritis. *Nat Rev Rheumatol* 2021;**17**:270−90.
4. Gorter SL, Bijlsma JW, Cutolo M, Gomez-Reino J, Kouloumas M, Smolen JS, et al. Current evidence for the management of rheumatoid arthritis with glucocorticoids: a systematic literature review informing the EULAR recommendations for the management of rheumatoid arthritis. *Ann Rheum Dis* 2010;**69**:1010−4.
5. Richards JS, Dowell SM, Quinones ME, Kerr GS. How to use biologic agents in patients with rheumatoid arthritis who have comorbid disease. *BMJ* 2015;**351**:h3658.
6. Li YF, Liang QW, Zhou LY, Cao YJ, Yang JY, Li J, et al. An ROS-responsive artesunate prodrug nanosystem co-delivers dexamethasone for rheumatoid arthritis treatment through the HIF-1α/NF-κB cascade regulation of ROS scavenging and macrophage repolarization. *Acta Biomater* 2022;**152**:406−24.

7. Kim T, Suh J, Kim WJ. Polymeric aggregate-embodied hybrid nitric-oxide-scavenging and sequential drug-releasing hydrogel for combinatorial treatment of rheumatoid arthritis. *Adv Mater* 2021;**33**:e2008793.
8. Liang HY, Peng B, Dong C, Liu LX, Mao JJ, Wei S, et al. Cationic nanoparticle as an inhibitor of cell-free DNA-induced inflammation. *Nat Commun* 2018;**9**:4291.
9. Fearon U, Canavan M, Biniecka M, Veale DJ. Hypoxia, mitochondrial dysfunction and synovial invasiveness in rheumatoid arthritis. *Nat Rev Rheumatol* 2016;**12**:385−97.
10. Tsai CH, Chen CJ, Gong CL, Liu SC, Chen PC, Huang CC, et al. CXCL13/CXCR5 axis facilitates endothelial progenitor cell homing and angiogenesis during rheumatoid arthritis progression. *Cell Death Dis* 2021;**12**:846.
11. Bartok B, Firestein GS. Fibroblast-like synoviocytes: key effector cells in rheumatoid arthritis. *Immunol Rev* 2010;**233**:233−55.
12. Prakken BJ, Samodal R, Le TD, Giannoni F, Yung GP, Scavulli J, et al. Epitope-specific immunotherapy induces immune deviation of proinflammatory T cells in rheumatoid arthritis. *Proc Natl Acad Sci U S A* 2004;**101**:4228−33.
13. Yang Z, Shen Y, Oishi H, Matteson EL, Tian L, Goronzy JJ, et al. Restoring oxidant signaling suppresses proarthritogenic T cell effector functions in rheumatoid arthritis. *Sci Transl Med* 2016;**8**:331ra38.
14. Khojah HM, Ahmed S, Abdel-Rahman MS, Hamza AB. Reactive oxygen and nitrogen species in patients with rheumatoid arthritis as potential biomarkers for disease activity and the role of antioxidants. *Free Radic Biol Med* 2016;**97**:285−91.
15. Jang D, Murrell GAC. Nitric oxide in arthritis. *Free Radic Biol Med* 1998;**24**:1511−9.
16. Chen CJ, Yin Y, Shi GN, Zhou Y, Shao S, Wei YZ, et al. A highly selective JAK3 inhibitor is developed for treating rheumatoid arthritis by suppressing γc cytokine-related JAK-STAT signal. *Sci Adv* 2022;**8**:eabo4363.
17. Ni RR, Song GJ, Fu XH, Song RF, Li LL, Pu WD, et al. Reactive oxygen species-responsive dexamethasone-loaded nanoparticles for targeted treatment of rheumatoid arthritis *via* suppressing the iRhom2/TNF-α/BAFF signaling pathway. *Biomaterials* 2020;**232**:119730.
18. Kim T, Suh J, Kim WJ. Polymeric aggregate-embodied hybrid nitric-oxide-scavenging and sequential drug-releasing hydrogel for combinatorial treatment of rheumatoid arthritis. *Adv Mater* 2021;**33**:2008793.
19. Wang Q, Zhou X, Yang L, Zhao YJ, Chew ZH, Xiao J, et al. The natural compound notopterol binds and targets JAK2/3 to ameliorate inflammation and arthritis. *Cell Rep* 2020;**32**:108158.
20. Lee Y, Kim H, Kang S, Lee J, Park J, Jon S. Bilirubin nanoparticles as a nanomedicine for anti-inflammation therapy. *Angew Chem Int Ed Engl* 2016;**55**:7460−3.
21. Hu J, Whittaker MR, Duong H, Li Y, Boyer C, Davis TP. Biomimetic polymers responsive to a biological signaling molecule: nitric oxide triggered reversible self-assembly of single macromolecular chains into nanoparticles. *Angew Chem Int Ed Engl* 2014;**53**:7779−84.
22. Vanslambrouck S, Riva R, Ucakar B, Préat V, Gagliardi M, Molin DGM, et al. Thiol-ene reaction: an efficient tool to design lipophilic polyphosphoesters for drug delivery systems. *Molecules* 2021;**26**:1750.
23. Liu R, Yu MN, Yang XT, Umeshappa CS, Hu C, Yu WQ, et al. Linear chimeric triblock molecules self-assembled micelles with controllably transformable property to enhance tumor retention for chemo-photodynamic therapy of breast cancer. *Adv Funct Mater* 2019;**29**:1808462.
24. Ma YX, Lu ZW, Jia B, Shi Y, Dong J, Jiang SX, et al. DNA origami as a nanomedicine for targeted rheumatoid arthritis therapy through reactive oxygen species and nitric oxide scavenging. *ACS Nano* 2022;**16**:12520−31.
25. Guo LN, Zhong SH, Liu P, Guo M, Ding JS, Zhou WH. Radicals scavenging mofs enabling targeting delivery of sirna for rheumatoid arthritis therapy. *Small* 2022;**18**:2202604.
26. Stahl S, Davies MR, Cook DI, Graham MJ. Nuclear hormone receptor-dependent regulation of hepatic transporters and their role in the adaptive response in cholestasis. *Xenobiotica* 2008;**38**:725−77.
27. Nagy L, Szanto A, Szatmari I, Széles L. Nuclear hormone receptors enable macrophages and dendritic cells to sense their lipid environment and shape their immune response. *Phys Rev* 2012;**92**:739−89.
28. Liu L, Hu FL, Wang H, Wu XL, Eltahan AS, Stanford S, et al. Secreted protein acidic and rich in cysteine mediated biomimetic delivery of methotrexate by albumin-based nanomedicines for rheumatoid arthritis therapy. *ACS Nano* 2019;**13**:5036−48.
29. Kan SY, Duan MM, Liu Y, Wang CL, Xie J. Role of mitochondria in physiology of chondrocytes and diseases of osteoarthritis and rheumatoid arthritis. *Cartilage* 2021;**13**:1102s−21s.
30. Yeo JW, Lee YM, Lee J, Park D, Kim K, Kim J, et al. Nitric oxide-scavenging nanogel for treating rheumatoid arthritis. *Nano Lett* 2019;**19**:6716−24.
31. Kasten TP, Collin-Osdoby P, Patel N, Osdoby P, Krukowski M, Misko TP, et al. Potentiation of osteoclast bone-resorption activity by inhibition of nitric oxide synthase. *Proc Natl Acad Sci U S A* 1994;**91**:3569−73.
32. Zhang L, Chen X, Cai PQ, Sun H, Shen SY, Guo BS, et al. Reprogramming mitochondrial metabolism in synovial macrophages of early osteoarthritis by a camouflaged meta-defensome. *Adv Mater* 2022;**34**:2202715.